Research Article

Fevzican Durmuş, Ferid Salehli, Murat Yazıcı* and Ali Gelir

Effect of pressing temperature on β-phase ratio of electrospun PVDF

https://doi.org/10.1515/epoly-2025-0046
Received July 14, 2025; accepted October 5, 2025;
published online February 3, 2026

Abstract: In this study, the morphological evolution of electrospun PVDF during hot compression for piezoelectric sensor production is investigated. The work assesses how compression alters total crystallinity, structural relaxation, and partial crystalline forms known as Form II, I, and III (α, β, and γ phases), including transitions among these forms. Relaxation in amorphous and crystalline regions, together with stress-induced melting, produces changes in phase distribution. FTIR, XRD, and DSC measurements show a reduction in the absolute fraction of the beta phase. Changes in dielectric spectra confirm a decline in ordered beta and indicate a corresponding increase in amorphous fraction as compression temperature rises. The method used here enables identification of a threshold compression temperature at which electrospun PVDF samples achieve minimal porosity while preserving the high long-range order of the beta phase. These results guide optimization of conditions and support robust, device-relevant functional performance in PVDF-based piezoelectric sensors.

Keywords: PVDF; electrospinning; nanofiber; relaxations; phase transitions

1 Introduction

Polyvinylidene fluoride (PVDF) is a common polymer that is used in piezoelectricity needed working areas such as pressure sensors, actuator electronics, etc. [1]. The most challenging factors of this material are the production method, service conditions, and continuity of its properties. Production techniques and further processes determine the piezoelectric properties of PVDF. Every process has different resulting crystalline forms of semi-crystalline PVDF polymer. It has many different crystalline sub-forms but is mostly known as Form I (ß-phase), Form II (α-phase), and Form III (γ-phase) [2, 3]. PVDF tends to be in Form II in normal conditions, especially when the melt processes produce it [4–6]. Form II is the more stable form in terms of energies but has no significant piezoelectric properties due to its TGTG' (T = Trans, G = Gauche) formation [5, 7, 8]. As in the steric structures of different forms of PVFD can be seen in Figure 1, the dipole moments between F- and H-groups are scattered randomly, and with that TGTG' formation, the overall dipole moment results in lower values, even at zero. Some external processes can be applied to Form II, and the piezoelectric effect can be obtained, such as polarization [9], stretching [6, 10, 11], and compressing [12–15], with special conditions. Still, continuity and material durability become secondary problems at that point. So, other forms like I or III must be considered for the continuous piezoelectric behavior of the material.

There are several ways to obtain PVDF in Form I and III, such as nucleating additives [16, 17] and solvent casting processes [18–20]. In particular, nanoparticles that have conductivity and ferroelectricity have tangible contributions to acquiring electroactive phases. In neat PVDF cases, solvent-included methods like spin coating [18] and electrospinning [4, 21] are common methods to get Form III and especially Form I. The main concern of electroactive phases is arranging final dipole moments and preventing them from being anti-parallelized by one another. The TTTT planar zigzag formation of Form I and the similar formation of Form III bring a resultant dipole moment magnitude far different from zero [22, 23].

Electrospinning is the proven method [24, 25] to obtain a high ratio of Form I PVDF. External electric field application during the production method gives the PVDF molecules a guide in solution form to be deposited on the rotary collector in an oriented formation. Dispersing polymer chains in a solvent, which is the first step of the electrospinning process, increases the ability of alignment of polymer chains. Needle-like nozzle systems inject the polymer solution via pumping with the help

***Corresponding author: Murat Yazıcı**, Automotive Engineering Department, Bursa Uludağ University, Bursa, Türkiye,
E-mail: myazici@uludag.edu.tr. https://orcid.org/0000-0002-8720-7594
Fevzican Durmuş, Automotive Engineering Department, Bursa Uludağ University, Bursa, Türkiye. https://orcid.org/0009-0005-9735-3287
Ferid Salehli and Ali Gelir, Physics Engineering Department, Istanbul Technical University, Istanbul, Türkiye

Open Access. © 2025 the author(s), published by De Gruyter. This work is licensed under the Creative Commons Attribution 4.0 International License.

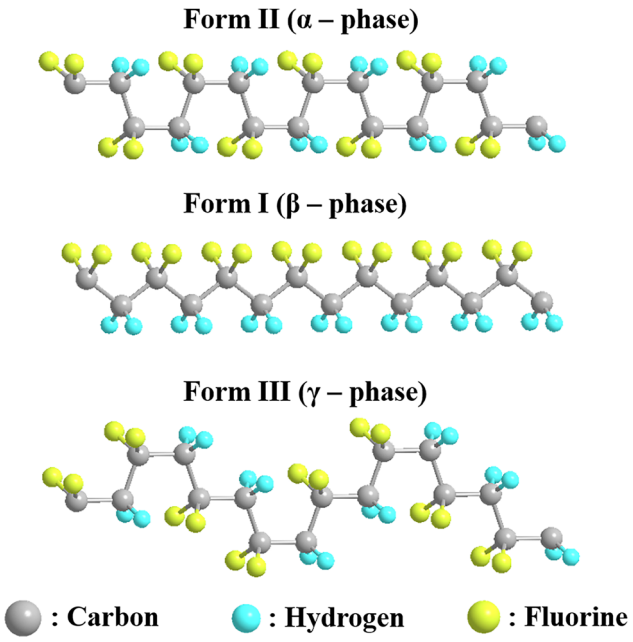


Figure 1: Schematic representation of PVDF phases.

of a potential difference applied between the nozzle and the collector side. Potential difference enhances the polarization of polymer chains. It aligns –F and –H groups more in planar zigzag form with the effect of the electric field, helping to get PVDF in Form I [26]. The nozzle creates a Taylor cone, and the polymer solution travels as a nanofiber and deposits on the collector in a mat form, which rotates simultaneously to provide homogeneity and continuity of nanofibers in the final sample [27]. The uniformity of nanofibers is directly proportional to the Form I phase amount and quality. The main parameters to obtain advanced nanofiber form and better piezoelectric final properties are the solution ratio, pumping rate, potential difference, nozzle-collector distance, and rotation rate of the collector. All the parameters above affect the shape of the Taylor cone, and so the fiber properties, such as existence, diameter, porosity, and alignment, are determined.

Electrospinning of PVDF has many advantages in getting a higher Form I phase ratio compared to other methods and piezoelectric properties, but it does not have the highest crystalline amount and the harmony of crystalline sites for the semi-crystalline structure of the polymer. The nanofiber structure and the existence of solvents in the method cause porosity in the final sample. Even if the pumping rates are meager, the solvent or solvent mixture may not find enough time to evaporate. Additional treatments can be applied to eliminate the residual solvents and porosity that are induced by solvent residue. Physical entanglement of nanofibers is another reason that disables the compaction of nanofibers if they cross one another. Annealing treatment gives some relaxation to the material, but the elevated annealing temperatures allow for the deformation of Form I into another form [28]. Pressure application is a possible way to reorder the inner structure of the electrospun PVDF. Temperature increment helps to move amorphous areas and crystalline side areas more easily [6, 13]. Even though there are so many positive factors that make electrospinning usage for the production of PVDF, final samples have some drawbacks in industrial usage because of their porosity and electrostatic surface. The porosity of the samples coming from the nanofiber structure can also be reduced via optimal pressing temperature, and reordering the inner structure via beating electrostatic forces can make the final sample easier to use during sensor production. Also, sandwiching during sensor production needs hot pressing to ensure electrodes and the main PVDF layer stick together. Elevated pressing temperature may cause a drop in performance in the sensor. Surface coating machines also use little pressure and high temperature to enhance good bonding. These kinds of short-time heating applications are affecting the final properties of PVDF-based piezoelectric sensors.

This paper investigates the effect of pressing and additional heating temperature during the pressing of electrospun PVDF in terms of total crystalline amount, Form I phase ratio, morphology, and dielectric properties.

2 Materials and methods

The Electrospinning method is used to obtain thin-film polymers with nanofiber structures. PVDF is used in powder form to ease dissolution, supplied from Sigma Aldrich, with CAS number: 24937-79-9. DMF and Acetone solvents are supplied from Tekkim Kimya, Turkey.

As our early study reveals [21], to dissolve 15 % PVDF powder by weight, a 6:4 DMF/Acetone ratio solvent is used during electrospinning. The solution is stirred in a magnetic stirrer overnight at room temperature to obtain better dispersion of polymer chains into the solvent, which enables more homogeneous nanofibers. A 15 kV high voltage is applied to the system with a needle-collector distance of 15 cm. The syringe pump speed is set at 1 mL/h during the process.

The obtained polymer film is divided into 6 equal parts, each one measuring 55 mm wide. Divided parts are dried in a vacuum oven at 40 °C for 6 h to eliminate humidity before pressing, and so water bubbles, if any. Pressing temperatures are selected around Vicat softening temperature [29] and a relaxation region [30] of PVDF around 80 °C. Temperatures are set as 40, 60, 80, 100, and 120 °C, and samples are named P1, P2, P3, P4, and P5, respectively, as can be seen in Table 1. As a pressing template, high-surface-finished

Table 1: Sample nomenclature.

	Press temperature
Unpressed	–
P1	40 °C
P2	60 °C
P3	80 °C
P4	100 °C
P5	120 °C

aluminum discs with a 50 mm diameter are used. Between two templates, poly(tetrafluoroethylene) based Teflon® films are used as release sheets. Between two release sheets, PVDF samples are placed which are about to be pressed.

Heating is carried out with disc patterns before samples are placed. After the desired temperature is obtained, the sample is placed between sheets, and 5 tons of force is applied via 50 mm diameter disc patterns (which equals ~24.68 MPa pressure) for 10 min. After pressing, the sample is taken with Teflon® sheets and cooled at room temperature. The final samples pressed can be seen in Figure 2.

Fourier Transform Infrared (FT-IR) spectroscopies of samples are measured to find peaks at specific wavenumbers that give an impression of the steric structure and configuration of atoms at some points. Spectra are taken with the Shimadzu IRTracer-100 device.

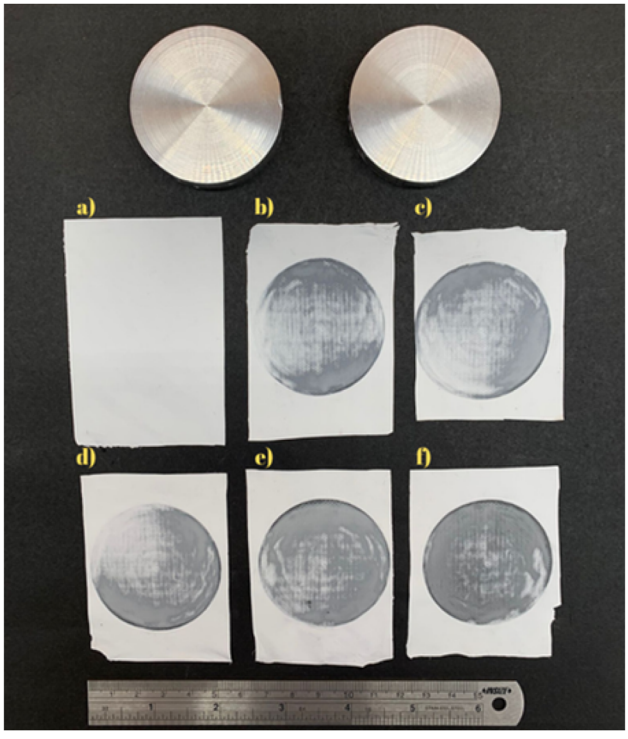


Figure 2: Press templates (upper side) and samples after pressure application (a) unpressed, (b) P1, (c) P2, (d) P3, (e) P4, (f) P5.

X-ray diffraction behavior of the samples is observed to see the crystalline planes of the samples. Different crystalline forms have specific plane orientation combinations, and Wide-Angle X-Ray Diffraction (WAXD) characterization helps to characterize those planes and crystalline forms. WAXD patterns are taken with a Bruker AXS/Discovery D8 diffractometer device, monochromatic CuKα (λ = 1.54060 Å) radiation by changing 2θ from 5° to 40° with a 0.02° step.

Observation of the total crystalline amount of the polymeric system and investigation of compaction of crystalline sites are carried out with Differential Scanning Calorimetry (DSC). The 5 mg sample is used in DSC measurement at 10 °C/min heating rate within 20–220 °C temperature range in N_2 atmosphere. Shape, location, and area of the melting peak, and the onset point, demonstrate the characteristics of the samples. DSC analysis is held with the TA Instrument DSC 25 model device.

Monitoring the change of crystalline structure and nanofiber orientations are critical for changing temperatures. The Scanning Electron Microscopy (SEM) method is used to see the morphological changes of pressed samples. All samples are coated with Au/Pd (60/40 % wt.) with a Bal-Tec SCD005 sputter coater to be prepared for scanning electron microscopy. SEM characterization is performed using the ZEISS EVO40 device for each sample in a vacuum.

Dielectric spectra of real (ε') and imaginary (ε'') parts of PVDF samples were measured at room temperature in the frequency range of 102 Hz–107 Hz using Novocontrol Alpha Analyzer (Concept-80). Samples with a thickness of 30 μm and a diameter of 8 mm were metallized in the form of flat parallel-plate capacitors using a pressed thin aluminum lamella. The best fitting of the dielectric loss spectra was performed by means of Havriliak-Negami (HN) relation [31] where $\Delta\varepsilon_k$ is the relaxation strength of successive relaxation processes, τ_{ok} denotes the relaxation times of the corresponding relaxation process, ε_∞ is the high frequency limit of dielectric constant, a and b exponents ($0 \le a, b \le 1$) are the shape parameters. The conductivity term, $\sigma_o(iw)^{(-s)}$, was omitted since the value $\sigma_o \approx 10^{-14}$ S/cm of samples can be neglected at room temperature.

$$\varepsilon^*(w) - \varepsilon_\infty = \sum_k \frac{\Delta\varepsilon_k}{\left[(1 + (iw_k\tau_{ok}))^a\right]^b} \quad (1)$$

3 Results

Even if the samples have the same elemental existence, changing bond angles and differential vibrations of varying

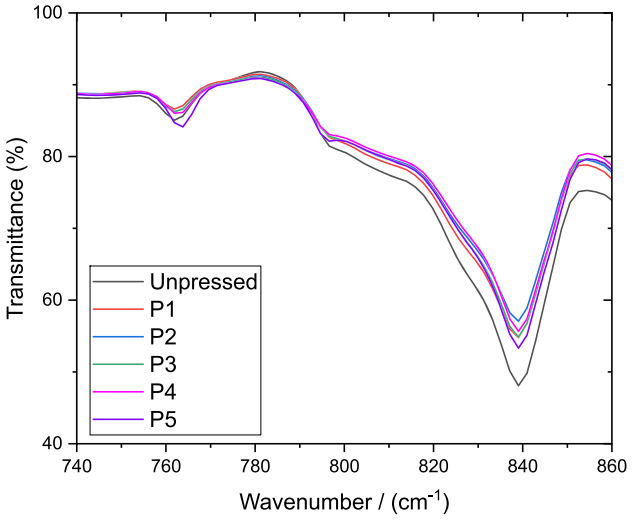


Figure 3: FT-IR spectrum of samples between 740 and 860 cm^{-1} wavenumbers.

PVDF forms can be distinguished by different methods such as FT-IR spectroscopy [2, 32]. Figure 3 shows the infrared spectrum of samples between 740 and 860 cm^{-1} wavenumber.

Each sample shows a significant peak at 840 cm^{-1} which is a solid sign of Form I phase existence [33–35]. Also, at 766 cm^{-1}, there is a clear sign of Form II phase, for each sample with varying percentages. The ratio of Form I can be calculated for each sample using an equation used by Osaki [36] and derived by Gregorio Jr. [37] for the PVDF polymer. Absorbance values at 766 and 840 cm^{-1} in Eq. (2) to calculate Form I phase ratio [$F(ß)$] for each sample.

$$F(ß) = \frac{A_ß}{1.262A_\alpha + A_\beta} \quad (2)$$

As can be seen in Table 2, the unpressed electrospun sample has the highest Form I phase ratio. With the effect of pressing, Form I ratio of P1 and P2 is slightly decreasing during the residual stress discharging of nanofibers. After reaching 80 °C in P3, Form I ratio starts decreasing more significantly since there are two transition-like relaxations between 60 and 100 °C, first one is at around 60 °C, which is related to amorphous region and folding behavior of groups in the polymer chain [32]. The other one is αc relaxation, around 90–100°, which includes movement and rotation of molecular groups and changing the directions of dipoles, also reordering around crystalline regions [30, 32, 38]. This transformation can also be seen as Vicat softening point, which is a more industrial aspect of polymers, around 80 °C for PVDF. Morphological transitions are about the close-packing behavior of crystalline areas of polymers, neither staying solid nor melting or deforming. Bond behavior

Table 2: ß phase ratios by Eq. (1).

	$F(ß)$
Unpressed	73.35 %
P1	72.78 %
P2	72.33 %
P3	70.81 %
P4	71.55 %
P5	69.98 %

changes of polymeric structures are decisive for certain temperature studies and the reorganization movements of polymer molecules at those certain temperatures can help to get the desired semi-crystalline phase structure conformations. Those transformations are the main reason for losing some of Form I crystalline after that point. They tended to be reordered and be more in Form III and Form II and in amorphous form after gaining some mobility and relaxation. At wavenumber 795 cm^{-1}, a slight increase of P5 shows transition to Form II phase which can be seen at Figure 3.

There is another comparison at spectrum between 450 and 550 cm^{-1}, having significant proofs of crystalline transitions. As can be seen in Figure 4, increase at around 485 cm^{-1} for P3, P4 and P5 shows amorphous transition of Form I crystallines clearly. Also, the peak at 469 cm^{-1} can be seen more definite in P3, P4 and P5. Loss of 480 cm^{-1} peak, which indicates Form I phase, for those 3 samples sharpens the look of 469 cm^{-1} peak and transition become more visible at spectrum [4].

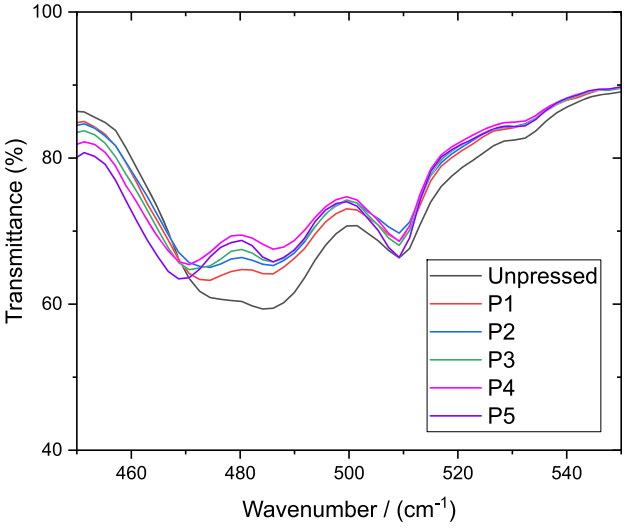


Figure 4: FT-IR spectrum of samples between 450 and 550 cm^{-1} wavenumbers.

FTIR is used only to compare ratios of crystalline phases. For precise quantitative results, FT-IR analysis alone is misleading. In this paper, to obtain the absolute Form I phase ratio, XRD and DSC characterization methods are used together to investigate semi-crystalline structure. In ordinary crystal solids, there must be several very sharp peaks and a planar baseline of near-zero intensity. However, in polymers, peaks become wider, and the baseline becomes higher and distorts since polymers are semi-crystalline, with amorphous regions [39]. Figure 5a shows the XRD pattern of the samples between 15° and 40° 2θ angles. There are 3 significant peaks in XRD pattern, each of them referring to planes of crystalline sites. Peaks at 34.51° and 22.89° and 20.5° represents the Form I phase (310, 020), (001) and (110, 200) planes respectively. [2, 40–42]. The lack of clarity of peak at 22.89° is the result of overlapping with planes of γ phase crystallines. The significant indicator peak of phase transformation is at 20.69° representing (110) plane for Form II phase, similar studies have this shift with compression [43]. As can be clearly seen in Figure 5b, Unpressed, P1, and P2 samples have peaks at around 20.5°, which are related to Form I. With the increasing pressing temperature, P3, P4, and P5 samples have those peaks different from others, higher intensities at around 20.7°, indicating transformation to Form II, correlatively with the FT-IR spectrum.

At lower temperatures, compression cannot beat the compaction of crystalline areas and the energy required to rotate bonds, and so cannot anticipate any transition. However, after the relaxation of molecular groups of crystalline and amorphous surroundings, it slightly mobilizes and tends to be in more steady states. Since Form II is a more stable phase, thermal applications at higher temperatures triggers phase transitions and metastable Form I phase bindingly [6, 32].

The movement capability of crystalline regions and the rotating facility of functional groups are highly dependent on the compaction of crystalline regions. For instance, α_a relaxation of PVDF samples is directly related to the segmental amorphous movement, which defines a glass transition [32]. For temperatures above 60 °C, α_c relaxation is dependent more on crystalline regions and their surroundings. Therefore, the total crystalline ratio is critical for those relaxations and phase transitions.

Like other vinyl-based polymers, PVDF has a restricted and controllable crystalline ratio of around 45–50 % by weight at most, for the melt crystallization [7]. When the optimal Taylor cone and nanofibers are formed, the electrospinning process gives much more limited crystallinity since the movement of polymer chains is restricted within the nanofiber diameter [4, 44]. This situation helps to get PVDF in the Form I phase more because of the hindrance coming from the smaller movement area and the electric field forces. But the total crystalline sites become much smaller than those of melt crystallization methods due to the restriction of the nanofiber diameter. The pumping ratio, needle diameter, and polymer concentration of the solvent are the main parameters to change nanofiber diameter, so the total crystalline ratio can be changed if needed [26]. In this work, all samples are separated from the same batch of the electrospinning process; therefore, the initial crystalline ratios are equal. The effect of pressing temperature on the crystallinity ratio of PVDF can be seen for those samples. DSC experiments show the total crystalline ratio change and the compaction of crystalline sites clearly in Figure 6.

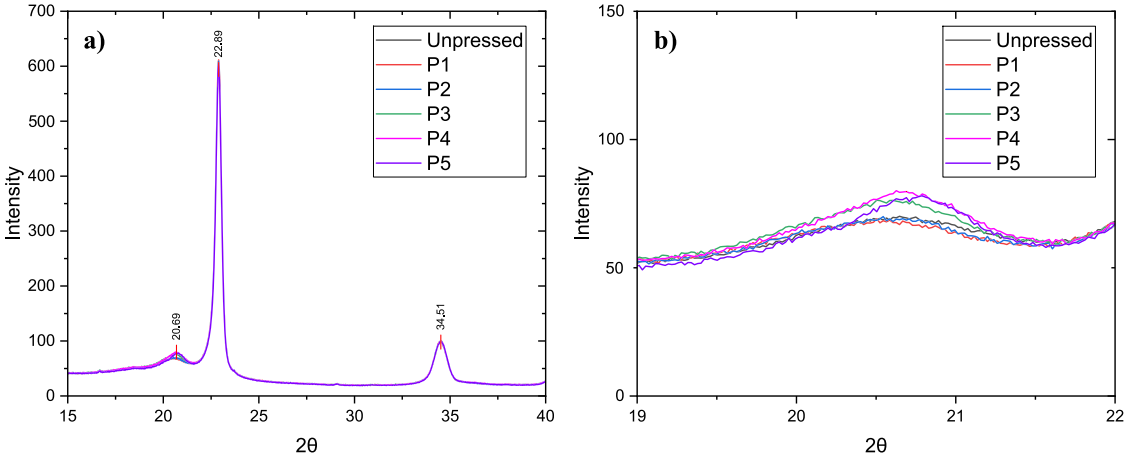


Figure 5: XRD patterns of samples (a) whole pattern, (b) zoom into 19°–22° region.

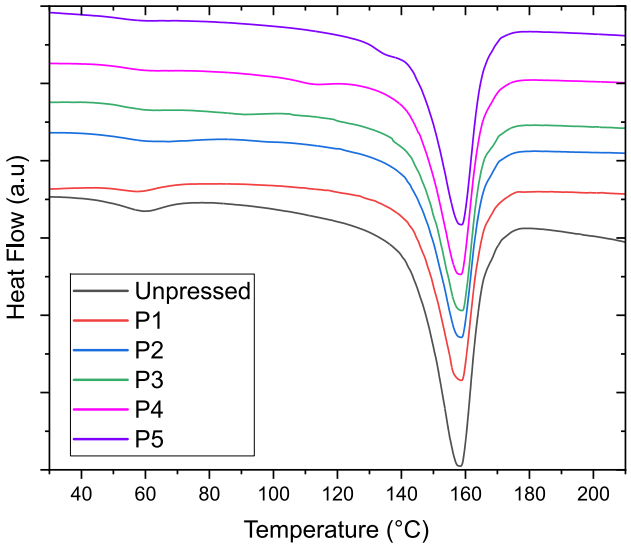


Figure 6: DSC measurements of all samples.

The plot shows DSC thermograms of the samples between 20 and 220 °C. Total crystallinity ratio X_c is calculated with Eq. (3) [37, 45]. ΔH_0 is used as 104.6 J/g [19, 28, 46]. The onset points are calculated directly from the TA Universal Analysis software program of the DSC device.

$$X_c = \frac{\Delta H_{peak}}{\Delta H_0} \times 100 \tag{3}$$

For almost all samples except the unpressed one and P5, similar melting peaks are observed. Melting peaks are located in the same range for each sample, because there is no additional crystalline densification and significant deformation. As the temperature of compression increases, total crystallinity decreases due to deformation of loose areas of crystalline surroundings. The difference between the P2 and P3 samples shows us the unfolding behavior of polymer chains, resulting in a slight decrease in total crystalline ratio. But the critical point is the shape of the melting peak for the P5 sample, which tends to be in a double-peaked shape, demonstrating that some of the dominant Form I phase could have been transformed during 120 °C compression [15, 45]. Besides, the sharper shape of the melting peak of each sample shows more compacted crystalline sites [39], which is expected for the compressed or stretched samples [47]. Loose crystalline areas can be compacted, and crystallizable amorphous sites may be slightly cold crystallized locally during the 120 °C compression, but since the deformation of the metastable Form I phase is the dominant parameter at 120 °C, the total X_c ratio change decreases markedly. Deformation of crystalline packing behavior before the actual melting point, with the high temperature relaxations and compression, results in X_c drop. Since there is no re-crystallization during this behavior, reordering of the crystalline structure and permanent phase transitions are observed [48].

Table 3: Crystallinity, Melting Point and Onset Temperature values from DSC characterization.

	X_c (%)	$X_ß$ (ß absolute)	T_m (°C)	T_{onset} (°C)
Unpressed	5.35	3.93	158.60	144.55
P1	4.20	3.06	158.82	145.07
P2	4.30	3.11	158.74	144.41
P3	4.22	2.99	158.92	144.49
P4	4.18	2.99	158.61	144.45
P5	4.19	2.93	158.93	145.12

Increase in the Form II phase fraction with decreased X_c can be explained with crystallization and transitions since the crystallizations above 100 °C result generally in Form II phase form [6, 15, 49]. Samples pressed at higher temperatures show less X_c because of loss of weak crystalline surroundings and deformation of less compacted crystalline sites.

The proximity of the onset point to the melting point shows the compaction of the crystalline region. That point generally has the same correlation with the changing melting temperature due to the effect of compression. Table 3 shows the X_c ratios, melting temperatures T_m, and onset temperatures T_{onset} of melting peaks.

The effect of pressing temperature to the crystalline structure is related with also the nanofiber diameters. The electric field makes the polymer chains stretch and arrange inside the restricted area, called a nanofiber. Polymer chains arrange inside solutions during deposition, then the solvent evaporates, and the final nanofibers are formed. But in case of lack of solubility, electric field cut off, clustering, loss of pumping rate, and high syringe-collector distance like factors, some beads can be formed [21, 26]. The difference between beads and nanofibers can be seen in Figure 7.

Those beads are different from nanofibers in terms of phase ingredients and physical properties. Since there is not enough force to align chains, generally a smaller amount of Form I phase exists inside beads compared to nanofibers because the stretch force of the electric field is less in beads, compared to thin nanofibers. Also, the nanofiber diameter is the main parameter that affects the electroactive phase quality at that point. The lower nanofiber diameter brings the higher electroactive properties to the final sample. Beads and thicker nanofibers have untight structures compared with thinner ones, which is why the nanofiber diameter is preferred as lower to obtain better piezoelectric properties. Unit cell volume of Form I is 2 times smaller than Form II and III crystalline [3, 22].

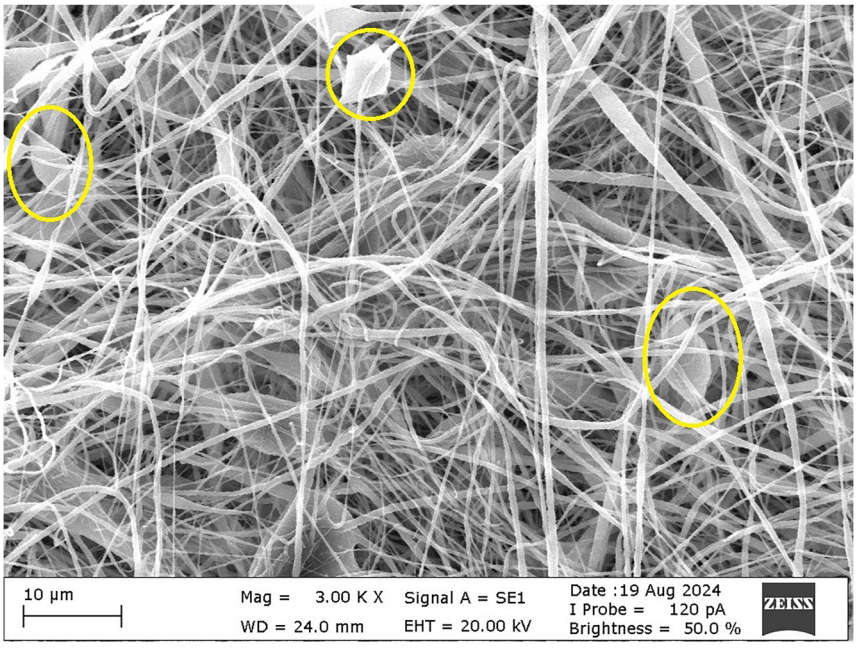


Figure 7: SEM image of unpressed sample at 3,000× magnification.

Distribution of nanofibers and beads in the microstructure can also affect the visual properties of the final samples, which can be seen in Figure 2. During the hot compress, beads and nanofibers squeeze in different ratios, and local opacities in the final sample can be observed. Increasing pressing temperature equalizes that ratio, and homogeneity in the visual aspect is obtained. Phase transformations are also dependent on this bead-nanofiber squeeze ratio. Reorientation of the PVDF chains is easier in beads, but nanofibers have much more resistance to transforming, especially as the nanofiber diameters decrease.

Nanofiber diameters are measured as ~270 nm for the unpressed sample and ~350 nm for P1 in the average random frame, which two still have measurable nanofibers. For samples P3 to P5, nanofiber formations are distorted as can be seen on SEM images in Figure 8 clearly.

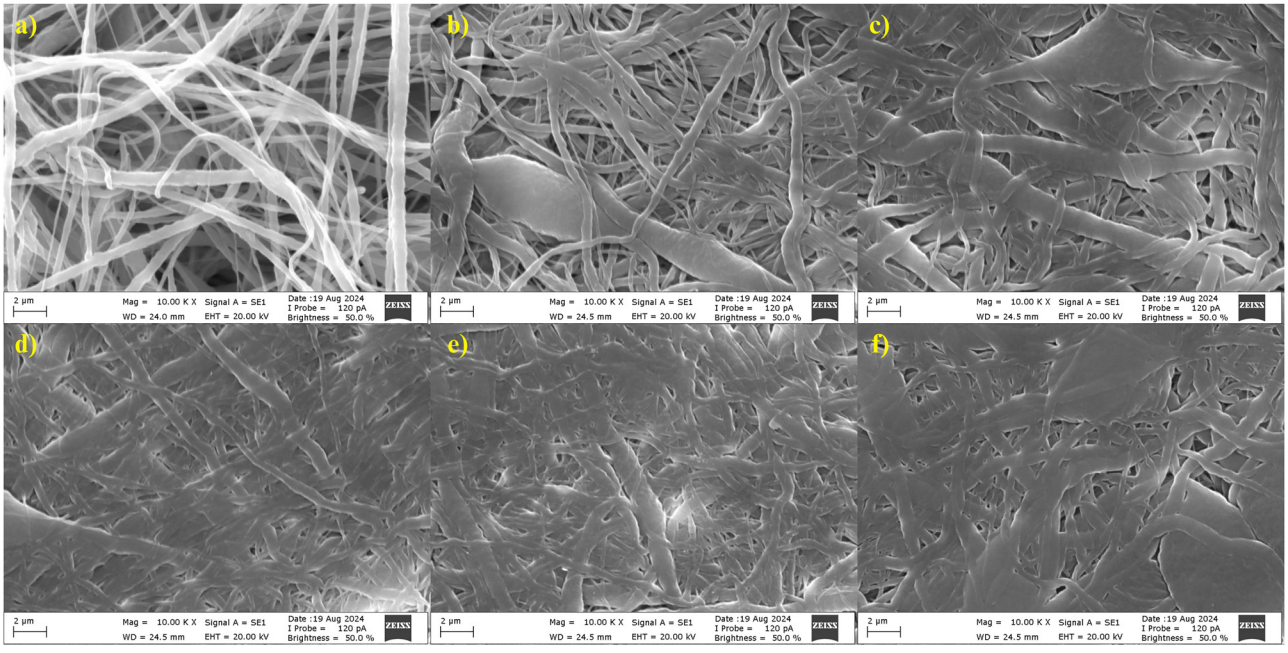


Figure 8: SEM images of whole samples at 10,000× magnification, (a) unpressed, (b) P1, (c) P2, (d) P3, (e) P4, (f) P5.

SEM images clearly show the change in the nanofiber structures depending on the pressing temperature. Deformations in the nanofiber profile of PVDF indicate the compaction and reorganization of the polymer sample. In Figure 8d and f, darker areas represent the complete deformation of the nanofiber structure and some of the Form I phase crystalline structure, via pressing and passing relaxation intervals, respectively. Especially after the P3, crystalline structure starts to transform and loses the tightness of the nanofiber formed crystalline structure, resulting in an electroactive property change.

Dielectric study of electrospun fibers of PVDF in the literature is rather scarce. To our best knowledge, only real permittivity spectra of PVDF fibers containing carbon nanotubes were discussed in [50]. Since the dielectric constant is proportional to the total molecular dipole moment, dielectric spectroscopy is an efficient tool for studying reorientational dynamics in various phases of polymeric materials. The FTIR results show that the maximum amount of ordered β-phase in unpressed PVDF decreases in pressed samples at elevated temperature (see Table 2). Similarly, XRD and DSC measurements indicate a decrease in the X_c crystallinity ratio of β-phase (Form I) with increasing pressing temperature (see Table 3). Figure 9 shows the dielectric spectra of unpressed and pressed PVDF samples at various temperatures. It is known that the molecular dynamics of the crystalline regions (α_c) is measured in the temperature dependence of dielectric loss, approximately at $T > 100$ °C [51]. Fitting of dielectric absorption spectra, using the HN formula given in Eq. (1), revealed the presence of two relaxation processes at all pressure temperatures of PVDF samples (Figure 9b). From the data presented in Table 3, it is obvious that the synthesized PVDF fibers contain mainly the amorphous phase. The high frequency dielectric loss around 10^6 Hz (Process I) is related to motions of dipolar amorphous segments (α_a) of residual stable α-phase crystallines (Form II), responsible for the low temperature glass transition [52]. The disordered state of the CH_2–CF_2 dipolar units relative to the II-order axis (C_{2v}) is apparently the reason for the noticeable $\varepsilon''(\omega)$ peak in Process I.

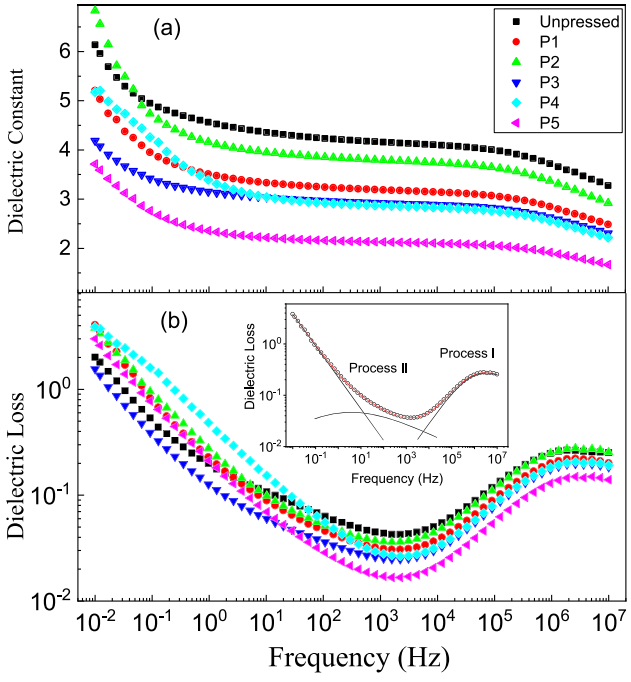


Figure 9: Real (a) and imaginary (b) dielectric spectra of unpressed and pressed PVDF samples when the temperature rises. In the inset, the example of the fitting procedure of ε'' (w) at 80 °C has been shown.

Comparing with data of previous studies of dielectric loss spectra at room temperature [52–54], the spectral position of Process II coincides with spectra associated with α_c-relaxation of crystalline chains. While the dipole contribution of the crystalline fraction to the $\varepsilon''(\omega)$ spectra is recorded as a remarkable peak in PVDF fibers, the Process II is measured with a view of broad response (inset in Figure 9b). For example, in a non-pressed sample, 5.35 % of the crystalline chains contain 3.93 % of the ordered β-phase (Table 3), the remaining parts are mostly in the amorphous phase. The low percentage of crystalline chains of different phases and their size distributions due to dispersion of fiber diameter is probably the reason for the broad loss response of dipoles in Process II. As can be seen from Figure 9a, an increase in pressing temperature of the samples leads to a decrease in the total dipole contribution to the susceptibility of PVDF in the entire spectral region. This is also confirmed by the fitting results of ε'' spectra presented in Table 4. Both the dielectric relaxation strength ($\Delta\varepsilon$) and relaxation times (τ) decreased with pressing temperature due to the diminishing of crystalline fraction and their sizes.

From the SEM images given in Figure 8, one can notice that porosity decreases with temperature, which leads to an

Table 4: Fitting parameters of ε'' spectra according to Havriliak-Negami formula.

	Process I		Process II	
	$\Delta\varepsilon$	τ (s) $\times 10^{-7}$	$\Delta\varepsilon$	τ (s) $\times 10^{-1}$
Unpressed	1.673	3.078	0.456	1.714
P1	1.114	1.802	0.299	2.997
P2	1.476	1.800	0.120	1.203
P3	0.994	1.455	0.159	1.591
P4	0.993	1.045	0.017	0.173
P5	0.718	1.089	0.068	0.683

increase in the density of pressed PVDF samples [15]. However, in polymers, relaxation times slow down exponentially with increasing density due to a decrease in free volume [55], while our finding indicates an opposite evolution of segmental relaxation times in PVDF. Thus, the decrease in relaxation times, i.e., faster motions of segments, points to a similarity of a "melting" effect in the PVDF, despite the fact that the density of pressed samples increases at elevated temperature. We would like to stress that the initiation of a high entropically state is not associated with real melting of PVDF since the d.c. conductivity of all samples, regardless of temperature, is about of $\sim 10^{-14}$ S/cm. The decrease of $\Delta\varepsilon$ (Table 4) in fast Process I indicates a gradual dipolar frustration of the crystalline areas. The emergence of dipole disordering will lead to the rendering of an amorphous phase in PVDF. According to XRD and DSC data, the ratio of crystallites decreases with pressing temperature (Table 3). It is anticipated that the short length scale amorphous phase is related to interphase regions between a crystalline and amorphous phase.

Changes in the dielectric parameters of the slow Process II point to the development of an amorphous state of the α-phase (Form II) with an increase in temperature of pressed samples. It can be assumed that the trend of molecular distortions of α-phase may lead to the development of a greater number of distorted molecules of γ-phase (Figure 1). Thus, the analysis of dielectric properties confirms the morphological changes of PVDF found in the above DSC, XRD, and FTIR studies.

4 Discussion

The main reason for phase transformation, which is enhanced by the bead formation and nanofiber enlargement, is the atomic structure of the PVDF crystalline. For two samples that have the same X_c, Form I phase structure has a higher density than the α phase structure, owing to unit cell dimensions. According to early studies, even if they have the same amount of polymer chains in one unit cell, the Form I unit cell volume is 2 times smaller than the Form II unit cell [22]. This situation also explains the reason for the easier formation of the Form II phase if all conditions are ordinary, such as no pressure or tensile stress. So that, if there are higher temperature conditions up to 60–80 °C, the nanofiber structure and Form I phase will start to reduce and tend to be energetically more stable on the Form II phase side. Above those temperatures, any kind of thermal application, such as annealing, affects the morphological structure and results in decreases in dielectric properties [56]. Pressure application is the reductant factor for this transformation, by holding tighter the structure, even if there is an ordered ß-phase decrease caused by the heat increment. Retaining some close packings lets unit cells stay smaller, and so polarization of the polymer chain stays the same due to hindrance. If there is much more transformation, like there is no pressure or tension during heating, the structure changes readily and bonds rotate, or tilt, so the total polarization and dipole moments decrease at the final. The results of the dielectric measurements agree with these conclusions. Pressure application at higher temperatures protects the structure from losing much more crystallinity and the Form I phase while gaining a less porous structure.

Electrospun and unpressed PVDF samples have very high electrostatic forces on themselves. This behavior relates to intermolecular and intramolecular van der Waals forces. In all forms, there are intermolecular and electrostatic attractions due to the steric structure of PVDF [2], but the planar zigzag structure of Form I brings much higher intermolecular van der Waals forces since hindrance is much higher due to stretching during electrospinning coming from the electric field. Excess pressure application overcomes those hindrances with the help of relaxations and transitions via compaction of molecules, and the intermolecular van der Waals attractions and intramolecular electrostatic forces decrease dramatically.

Even if there is no critical change in crystalline structure and phase fractions observed in infrared spectrums, X-ray patterns and calorimetric analysis, dielectric properties of the samples are showing importance of high temperature applications because of those transformation phenomena.

5 Conclusions

Electrospun PVDF samples have outstanding properties among other production types, such as spin coating, solution casting, and melting techniques. Besides, nanofiber formation during electrospinning is enhancing crystalline structure, and a high electric field is increasing the stretch of polymer chains, resulting in the development of ß phase amount.

Porosity and the lack of utilization capability of directly electrospun samples are the problems of those materials. The effect of compression with external heating on electrospun samples was investigated in terms of morphology, crystallinity, and dielectric properties. Transparent and white areas of samples show the porosity changes, which means that compression reduces the porosity of samples, as shown in the photographs given in Figure 2. All samples have a small crystalline ratio of around 4–5%, as shown in Table 3 by DSC. According to XRD and FT-IR characterizations, all

phases have solid α, ß and γ phases (Forms II, I, and III, respectively). The initial samples have 73.35 % ß-phase (Form I) ratio. It was found that pressure reduces the crystallinity for each sample with the phenomenon of stress-induced melting. The ß-phase ratio is slightly decreased after the P2 sample, which has 60 °C compression. Thus, 60 °C as the pressing temperature can be considered as the threshold temperature for the decrease in the absolute ratio of β-phase. Dielectric results have the same trend with morphological studies. The decrease in the dielectric relaxation strengths, as well as the shortening of the relaxation times of molecular motions in Process I, indicates a decrease in the ratio of the dipole order of the ß-phase with an increase in the pressing temperature.

Research funding: The authors would like to thank the Scientific and Technological Research Council of Turkey (TUBITAK) for their support through Project Number 123E588.

Author contribution: Fevzican Durmuş: Writing – original draft, Writing – review & editing, Research, Analysis & Characterization. **Ferid Salehli:** Writing – original draft, Methodology. **Murat Yazıcı:** Methodology, Writing – review & editing, Project Administration. **Ali Gelir:** Writing – original draft, Writing – review & editing, Analysis.

Conflict of interest: The authors declare no conflict of interest.

References

1. Kawai H. The piezoelectricity of poly (vinylidene fluoride). Jpn J Appl Phys 1969;8:975.
2. Hasegawa R, Kobayashi M, Tadokoro H. Molecular conformation and packing of poly(vinylidene fluoride). Stability of three crystalline forms and the effect of high pressure. Polym J 1972;3:591–9.
3. Hasegawa R, Takahashi Y, Chatani Y, Tadokoro H. Crystal structures of three crystalline forms of poly(vinylidene fluoride). Polym J 1972;3: 600–10.
4. Gasparini TM, Suman Bretas RE, da Silva AB, Gregorio J, R. Processing and characterization of oriented electrospun poly(vinylidene fluoride) mats. J Polym Sci B Polym Phys 2012;50:1304–11.
5. Martins P, Lopes AC, Lanceros-Mendez S. Electroactive phases of poly(vinylidene fluoride): determination, processing and applications. Prog Polym Sci 2014;39:683–706.
6. Matsushige K, Nagata K, Imada S, Takemura T. The II-I crystal transformation of poly(vinylidene fluoride) under tensile and compressional stresses. Polymer 1980;21:1391–7.
7. Broadhurst MG, Davis GT, McKinney JE, Collins RE. Piezoelectricity and pyroelectricity in polyvinylidene fluoride – a model. J Appl Phys 1978;49: 4992–7.
8. Lando JB, Olf HG, Peterlin A. Nuclear magnetic resonance and X-ray determination of the structure of poly(vinylidene fluoride). J Polym Sci Part A-1: Polym Chem 1966;4:941–51.
9. Kułek J, Pawlaczyk C, Markiewicz E. Influence of poling and ageing on high-frequency dielectric and piezoelectric response of PVDF-type polymer foils. J Electrost 2002;56:135–41.
10. da Silva AB, Wisniewski C, Esteves JVA, Gregorio R. Effect of drawing on the dielectric properties and polarization of pressed solution cast β-PVDF films. J Mater Sci 2010;45:4206–15.
11. Sencadas V, Gregorio Jr. R, Lanceros-Méndez S. α to β Phase transformation and microestructural changes of PVDF films induced by uniaxial stretch. J Macromol Sci B 2009;48:514–25.
12. Huang Z-X, Wang M-M, Feng Y-H, Qu J-P. β-Phase formation of polyvinylidene fluoride via hot pressing under cyclic pulsating pressure. Macromolecules 2020;53:8494–501.
13. Matsushige K. Pressure effect on phase transition in ferroelectic polymers. Phase Transitions 1989;18:247–62.
14. Mireja S, Khakhar DV. High β-phase PVDF films formed by uniaxial compression. Polymer 2024;293:126665.
15. Na H, Zhao Y, Zhao C, Zhao C, Yuan X. Effect of hot-press on electrospun poly(vinylidene fluoride) membranes. Polym Eng Sci 2008;48:934–40.
16. Ke K, Pötschke P, Jehnichen D, Fischer D, Voit B. Achieving β-phase poly(vinylidene fluoride) from melt cooling: effect of surface functionalized carbon nanotubes. Polymer 2014;55:611–19.
17. Sebastian MS, Larrea A, Gonçalves R, Alejo T, Vilas JL, Sebastian V, et al. Understanding nucleation of the electroactive β-phase of poly(vinylidene fluoride) by nanostructures. RSC Adv 2016;6: 113007–15.
18. Cardoso VF, Minas G, Costa CM, Tavares CJ, Lanceros-Mendez S. Micro and nanofilms of poly(vinylidene fluoride) with controlled thickness, morphology and electroactive crystalline phase for sensor and actuator applications. Smart Mater Struct 2011;20:087002.
19. Sencadas V, Gregorio Filho R, Lanceros-Mendez S. Processing and characterization of a novel nonporous poly(vinilidene fluoride) films in the β phase. J Non-Cryst Solids 2006;352:2226–9.
20. Zhao Z, Li J, Yuan X, Li X, Zhang Y, Sheng J. Preparation and properties of electrospun poly(vinylidene fluoride) membranes. J Appl Polym Sci 2005;97:466–74.
21. Güçlü H, Kasım H, Yazici M. Investigation of the optimum vibration energy harvesting performance of electrospun PVDF/$BaTiO_3$ nanogenerator. J Compos Mater 2023;57:409–24.
22. Lovinger AJ. Ferroelectric polymers. Science 1983;220:1115–21.
23. Ribeiro C, Costa CM, Correia DM, Nunes-Pereira J, Oliveira J, Martins P, et al. Electroactive poly(vinylidene fluoride)-based structures for advanced applications. Nat Protoc 2018;13:681–704.
24. He Z, Rault F, Lewandowski M, Mohsenzadeh E, Salaün F. Electrospun PVDF nanofibers for piezoelectric applications: a review of the influence of electrospinning parameters on the β phase and crystallinity enhancement. Polymers 2021;13:174.
25. Yee WA, Kotaki M, Liu Y, Lu X. Morphology, polymorphism behavior and molecular orientation of electrospun poly(vinylidene fluoride) fibers. Polymer 2007;48:512–21.
26. Gee S, Johnson B, Smith AL. Optimizing electrospinning parameters for piezoelectric PVDF nanofiber membranes. J Membr Sci 2018;563: 804–12.
27. Zhao K, Wang W, Yang Y, Wang K, Yu D-G. From taylor cone to solid nanofiber in tri-axial electrospinning: size relationships. Results Phys 2019;15:102770.
28. Nakagawa K, Ishida Y. Annealing effects in poly(vinylidene fluoride) as revealed by specific volume measurements, differential scanning calorimetry, and electron microscopy. J Polym Sci Polym Phys Ed 1973; 11:2153–71.

29. Bastida S, Eguiazábal JI, Nazábal J. The Vicat softening temperature as a method to assess the phase behaviour of amorphous polymer blends. Polym Test 1993;12:233–42.
30. Mano JF, Sencadas V, Costa AM, Lanceros-Méndez S. Dynamic mechanical analysis and creep behaviour of β-PVDF films. Mater Sci Eng A 2004;370:336–40.
31. Havriliak S, Negami S. A complex plane representation of dielectric and mechanical relaxation processes in some polymers. Polymer 1967;8: 161–210.
32. McBrierty VJ, Douglass DC, Weber TA. Nuclear magnetic relaxation and molecular motion in poly(vinylidine fluoride). J Polym Sci Polym Phys Ed 1976;14:1271–86.
33. Boccaccio T, Bottino A, Capannelli G, Piaggio P. Characterization of PVDF membranes by vibrational spectroscopy. J Membr Sci 2002;210:315–29.
34. Gregorio Jr. R. Determination of the α, β, and γ crystalline phases of poly(vinylidene fluoride) films prepared at different conditions. J Appl Polym Sci 2006;100:3272–9.
35. Salimi A, Yousefi AA. Analysis method: FTIR studies of β-phase crystal formation in stretched PVDF films. Polym Test 2003;22:699–704.
36. Osaki S, Kotaka T. Electrical properties of form III poly(vinylidene fluoride). Ferroelectrics 1981;32:1–11.
37. Gregorio Jr. R, Cestari M. Effect of crystallization temperature on the crystalline phase content and morphology of poly(vinylidene fluoride). J Polym Sci B Polym Phys 1994;32:859–70.
38. Linares A, Acosta JL. Tensile and dynamic mechanical behaviour of polymer blends based on PVDF. Eur Polym J 1997;33:467–73.
39. Young JR, Lovell PA. Introduction to polymers, 3rd ed. Boca Raton, FL: CRC Press; 2011.
40. Liu Y, Liu WG, Lin DB, Niu XL, Zhou S, Zhang J, et al. Fabrication and optical properties of transparent P(VDF-TrFE) ultrathin films. Nanomaterials 2022;12:588.
41. Lu G, Tian T, Wang Y. Advanced electrospinning technology applied to polymer-based sensors in energy and environmental applications. Polymers 2024;16:839.
42. Wan C, Bowen CR. Multiscale-structuring of polyvinylidene fluoride for energy harvesting: the impact of molecular-micro- and macro-structure. J Mater Chem A 2017;5:3091–128.
43. Esterly DM, Love BJ. Phase transformation to β-poly(vinylidene fluoride) by milling. J Polym Sci B Polym Phys 2004;42:91–7.
44. Kongkhlang T, Tashiro K, Kotaki M, Chirachanchai S. Electrospinning as a new technique to control the crystal morphology and molecular orientation of polyoxymethylene nanofibers. J Am Chem Soc 2008;130: 15460–6.
45. Brunengo E, Luciano G, Canu G, Canetti M, Conzatti L, Castellano M, et al. Double-step moulding: an effective method to induce the formation of β-phase in PVDF. Polymer 2020;193:122345.
46. Lovinger AJ. Developments in crystalline polymers. Appl Sci, London 1982;1:195–273.
47. Schick C. 2.31 – calorimetry. In: Matyjaszewski K, Möller M, editors. Polymer Science: A Comprehensive Reference. Amsterdam: Elsevier; 2012:793–823 pp.
48. Barbosa R, Mendes JA, Sencadas V, Mano JF, Lanceros-Méndez S. Chain reorientation in β-PVDF films upon transverse mechanical deformation studied by SEM and dielectric relaxation. Ferroelectrics 2003;294: 73–83.
49. Gregorio R, Ueno EM. Effect of crystalline phase, orientation and temperature on the dielectric properties of poly (vinylidene fluoride) (PVDF). J Mater Sci 1999;34:4489–500.
50. Sharma M, Srinivas V, Madras G, Bose S. Outstanding dielectric constant and piezoelectric coefficient in electrospun nanofiber mats of PVDF containing silver decorated multiwall carbon nanotubes: assessing through piezoresponse force microscopy. RSC Adv 2016;6: 6251–8.
51. Sencadas V, Costa CM, Moreira V, Monteiro J, Mendiratta SK, Mano JF, et al. Poling of β-poly(vinylidene fluoride): dielectric and IR spectroscopy studies. E-Polymers 2005;5. https://doi.org/10.1515/epoly.2005.5.1.10.
52. Sy JW, Mijovic J. Reorientational dynamics of poly(vinylidene fluoride)/poly(methyl methacrylate) blends by broad-band dielectric relaxation spectroscopy. Macromolecules 2000;33:933–46.
53. Bello A, Laredo E, Grimau M. Distribution of relaxation times from dielectric spectroscopy using Monte Carlo simulated annealing: application to α− PVDF. Phys Rev B 1999;60:12764–74.
54. Frübing P, Wang F, Wegener M. Relaxation processes and structural transitions in stretched films of polyvinylidene fluoride and its copolymer with hexafluoropropylene. Appl Phys A 2012;107:603–11.
55. Floudas G. 2.32 – dielectric spectroscopy. In: Matyjaszewski K, Möller M, editors. Polymer Science: A Comprehensive Reference. Amsterdam: Elsevier; 2012:825–45 pp.
56. Tiwari V, Srivastava G. Effect of thermal processing conditions on the structure and dielectric properties of PVDF films. J Polym Res 2014;21: 587.